Interface dynamics: Mechanisms of stabilization and destabilization and structure of flow fields

Snezhana I. Abarzhi[a,1], Daniil V. Ilyin[b], William A. Goddard III[b], and Sergei I. Anisimov[c]

Edited by Jisoon Ihm, Pohang University of Science and Technology, Pohang, South Korea, and approved June 12, 2018 (received for review January 29, 2018)

Interfacial mixing and transport are nonequilibrium processes coupling kinetic to macroscopic scales. They occur in fluids, plasmas, and materials over celestial events to atoms. Grasping their fundamentals can advance a broad range of disciplines in science, mathematics, and engineering. This paper focuses on the long-standing classic problem of stability of a phase boundary—a fluid interface that has a mass flow across it. We briefly review the recent advances in theoretical and experimental studies, develop the general theoretical framework directly linking the microscopic interfacial transport to the macroscopic flow fields, discover mechanisms of interface stabilization and destabilization that have not been discussed before for both inertial and accelerated dynamics, and chart perspectives for future research.

interface dynamics | phase boundary | Landau–Darrieus instability | Rayleigh–Taylor instability | interfacial mixing

Interfacial mixing and transport are nonequilibrium processes coupling kinetic to macroscopic scales (1). They commonly occur in fluids, plasmas, and materials over celestial events to atoms (2, 3). Their understanding has crucial importance for science, mathematics, and engineering as well as for technology, energy, and environment (1–4). In this paper, we focus on the long-standing problem of stability of a phase boundary (i.e., a fluid interface) (5, 6). By developing the general theoretical framework, we systematically study the interface stability and the flow fields' structure; discover mechanisms of stabilization and destabilization of the inertial and accelerated dynamics that have not been discussed in the earlier studies (5, 6); elaborate diagnostics that have not been identified before and that directly link microscopic transport at the interface to macroscopic fields in the bulk; and chart perspectives for future research. For the readers' convenience, technical details are given in *SI Appendix* for the corresponding sections.

Hydrodynamic instabilities and interfacial mixing control a broad range of processes in nature and technology at astrophysical and molecular scales under conditions of high- and low-energy densities (1–3). Inertial confinement fusion and light–material interaction, supernovae and molecular clouds, stellar convection and ionospheric plasma, reactive fluids and material evaporation, fossil fuel production and nanoelectronics—these are some examples of processes to which nonequilibrium interfacial dynamics is directly relevant (7–17). In realistic environments, the material transport is often characterized by sharply and rapidly changing flow fields and by relatively small effects of dissipation and diffusion. This leads to formation of discontinuities (interfaces) separating the flow nonuniformities (phases) at continuous (macroscopic) scales (1–3, 18–20).

For a far-field observer, two types of hydrodynamic discontinuities are usually considered—a front (with zero mass transport across it) and an interface (through which mass can be transported) (5). Their dynamics is analyzed in a continuous approximation and at length scales and timescales that are greater than characteristic scales induced by diffusion, dissipation, surface tension, and other stabilizing effects (5, 6, 11–15). The fluid phases are broadly defined: These can be distinct materials or a material with distinct thermodynamic properties. The material(s) may also experience a phase transition, a change in chemical composition, be out of thermodynamic equilibrium, and/or have a nondiffusive interfacial mass transport (1–21). To describe the multiphase flow, a boundary value problem is solved for

[a]Department of Mathematics and Statistics, The University of Western Australia, Crawley, Perth, WA 6009, Australia; [b]Materials and Process Simulation Center, California Institute of Technology, Pasadena, CA 91125; and [c]Landau Institute for Theoretical Physics, Russian Academy of Sciences, Chernogolovka 142432, Russia

Author contributions: S. I. Abarzhi designed research; S. I. Abarzhi and D.V.I. performed research; S. I. Abarzhi, D.V.I., W.A.G., and S. I. Anisimov analyzed the results and data; and S. I. Abarzhi, D.V.I., W.A.G., and S. I. Anisimov wrote the paper.

The authors declare no conflict of interest.

This article is a PNAS Direct Submission.

[1]To whom correspondence should be addressed. Email: snezhana.abarzhi@gmail.com.

This article contains supporting information online at www.pnas.org/lookup/suppl/doi:10.1073/pnas.1714500115/-/DCSupplemental.

balancing at a freely evolving discontinuity the fluxes of mass and normal component of momentum in case of fronts and the fluxes of mass, momentum, and energy in case of interfaces (5). While solving the boundary value problem can be a challenge, this level of abstraction has a number of advantages. On the side of fundamentals, the problem is treated rigorously, powerful theoretical methods [e.g., group theory (2)] are applied, and essentials of the dynamics are explored. On the side of applications, this approach provides reliable macroscopic benchmarks for diagnostics, is free from adjustable parameters, and has high predictive capability in a broad parameter regime (2, 3, 5, 20).

Dynamics of fronts separating fluids of different densities is usually neutrally stable and can be destabilized by accelerations and shocks, leading to the Rayleigh–Taylor (RT) and Richtmyer–Meshkov (RM) instabilities, respectively, and the ensuing interfacial mixing of the fluids (22–26). Rigorous theoretical approaches have been developed to describe RT and RM flows with account for the nonlocal anisotropic, heterogeneous, and statistically unsteady character of their dynamics (2, 3, 27–31). These approaches have captured the fundamental properties of the instabilities and mixing (including the multiscale RT/RM dynamics and the order in RT mixing) and have explained the observations (2, 3, 26, 30).

Dynamics of interfaces separating fluids of different densities and having an interfacial mass flux is a long-standing problem with a broad range of applications (5). It is studied in plasmas (stability of ablation fronts in inertial confinement fusion), astrophysics (thermonuclear flashes on the surface of compact stars), material science (material melting and evaporation), gas dynamics (shocks and explosions), combustion (stability of flames), and industry (scramjets) (6–16, 32–40). The classic theoretical framework for the problem was developed by Landau (40). It analyzes the dynamics of a discontinuous interface separating ideal incompressible fluids of different densities. By balancing at the interface the fluxes of mass and momentum and by implementing a special condition for the perturbed mass flux, this analysis finds the interface to be unconditionally unstable, leading to the Landau–Darrieus instability (LDI) (5, 6, 40).

To connect the classic framework (5, 40) to realistic environments, several approaches have been developed. In high-energy density plasmas, significant departures have been detected between the ablative RT and accelerated Landau–Darrieus (LD) instabilities as well as between the ablative RM and LD instabilities (32–35, 41–43). It has been recently shown that the interface stability is sensitive to the flux of energy fluctuations produced by the perturbed interface (20). In reactive and supercritical fluids, the stabilizing influences have been found of dissipation, diffusion, surface tension, and finite interface thickness on the dynamics at small scales (6, 11, 37–39). Significant progress has been achieved in the understanding of nonlinear stages of the LDI and in modeling of turbulent combustion (11, 44, 45). These theories and models have successfully expanded the classic framework (5, 40) to explain the observations (6, 11, 32–39, 41–46). However, some fundamental challenges remain.

First, the classic framework (5, 40) describes the evolution of a phase boundary and is relevant to a range of phenomena far beyond processes with gradually changing flow fields (1–16, 32–45). We still need to understand whether the interface is stable when the flow quantities experience sharp changes, the effect of dissipation and diffusion is negligible, and the interfacial transport is nondiffusive. Second, the flow evolution is usually observed from a far field and at timescales and length scales that are substantially greater that those induced by interfacial processes at small scales (6–20). We still need to quantify what the flow sensitivity is to the boundary conditions at the interface. Third, direct diagnostics of various physical effects on dynamics of a multiphase flow require detailed information of the interface structure. Such information is often a challenge to obtain directly in experiments and simulations (6–18, 32–46). We need to better comprehend what the qualitative and quantitative influence is of the interfacial transport at microscopic scales on volumetric flow fields at macroscopic scales and elaborate reliable benchmarks. This knowledge is necessary to identify the mechanisms of stabilization and destabilization of interfacial dynamics; to improve the diagnostics of complex processes in plasmas, fluids, and materials; and to better understand a broad range of phenomena in nature and technology (1–16).

In this paper, we consider from a far field the inertial and accelerated dynamics of a hydrodynamic discontinuity that separates ideal incompressible fluids of different densities and is accompanied by the interfacial mass flux. By generalizing the classic framework (5, 40), we link directly the interface stability to the flow fields' structure. Mechanisms are identified of the interface stabilization and destabilization that have not been discussed before. We find that the inertial dynamics is stable when it conserves the fluxes of mass, momentum, and energy; the stabilization is due to the inertial effect, leading to small oscillations of the velocity of the interface as a whole. An energy imbalance can destabilize the dynamics (20), which is fully consistent with the classic results (5, 40). In reactive fluids, the energy imbalance can be due to chemical reactions (4, 46). For accelerated dynamics, the interface stability is determined by the interplay of the effects of inertia and buoyancy. A hydrodynamic instability is found that has not been identified in earlier studies (5, 6, 11, 32–46) and that develops when the gravity value exceeds a threshold. This unstable dynamics conserves the fluxes of mass, momentum, and energy; has potential velocity fields in the bulk; and is shear-free at the interface. The qualitative, quantitative, and formal properties of this instability differ dramatically from those of the accelerated LDI and the Rayleigh–Taylor instability (RTI) (5, 22, 23, 40).

Theoretical Approaches

Governing Equations. Dynamics of ideal fluids is governed by the conservation of mass, momentum, and energy. In an inertial reference frame,

$$\partial\rho/\partial t+\partial\rho v_i/\partial x_i=0,\ \partial\rho v_i/\partial t+\sum_{j=1}^{3}\partial\rho v_i v_j/\partial x_j+\partial P/\partial x_i=0,\ \partial E/\partial t+\partial(E+P)v_i/\partial x_i=0, \quad [1a]$$

where x_i are the spatial coordinates with $(x_1, x_2, x_3)=(x, y, z)$; t is time; $(\rho, \mathbf{v}, P, E)$ are the fields of density ρ, velocity $\mathbf{v}$, pressure P, and energy $E=\rho(e+\mathbf{v}^2/2)$; and e is the specific internal energy (5).

We introduce a continuous local scalar function $\theta(x, y, z, t)$, with derivatives $\dot{\theta}$ and $\nabla\theta$ that exist (the dot denotes partial time derivative) such that the heavy (light) fluid marked with subscript $h(l)$ is located in the region $\theta>0$ ($\theta<0$), and the interface is at $\theta=0$ (2, 5, 20, 30, 31). We represent the flow fields in the entire domain as $(\rho, \mathbf{v}, P, E)=(\rho, \mathbf{v}, P, E)_h H(\theta)+(\rho, \mathbf{v}, P, E)_l H(-\theta)$, where $H(\theta)$ is the Heaviside step function. In the bulk of the heavy (light) fluid, $(\rho, \mathbf{v}, P, E)\to(\rho, \mathbf{v}, P, E)_{h(l)}$ in the governing equations. At the interface, the balances of fluxes of mass and of normal and tangential components of momentum and energy lead to the boundary conditions (5)

$$\left[\tilde{\mathbf{j}}\cdot\mathbf{n}\right]=0,\quad \left[\left(P+\left(\tilde{\mathbf{j}}\cdot\mathbf{n}\right)^2/\rho\right)\mathbf{n}\right]=0,\quad \left[\left(\tilde{\mathbf{j}}\cdot\mathbf{n}\right)\left(\left(\tilde{\mathbf{j}}\cdot\boldsymbol{\tau}\right)/\rho\right)\boldsymbol{\tau}\right]=0,\quad \left[\left(\tilde{\mathbf{j}}\cdot\mathbf{n}\right)\left(W+\tilde{\mathbf{j}}^2/2\rho^2\right)\right]=0. \quad [1b]$$

Here, $[...]=0$ denotes the jump of functions at the interface. $\mathbf{n}$ and $\boldsymbol{\tau}$ are the normal and tangential unit vectors, respectively, at

the interface with $\mathbf{n}=\nabla\theta/|\nabla\theta|$, $(\mathbf{n}\cdot\boldsymbol{\tau})=0$; $\tilde{\mathbf{j}}=\rho(\mathbf{n}\dot{\theta}/|\nabla\theta|+\mathbf{v})$ is the mass flux across the moving interface; and $W=e+P/\rho$ is the specific enthalpy. We use physics definitions of W, e (5, 20). For a spatially extended 2D flow propagating in the z direction, periodic in the x direction, $x+\lambda\to x$, and motionless in the y direction, the conditions at outside boundaries of the domain are

$$\mathbf{v}_h|_{z\to-\infty}=\mathbf{V}_h=(0,0,V_h),\quad \mathbf{v}_l|_{z\to+\infty}=\mathbf{V}_l=(0,0,V_l) \qquad [1c]$$

with constant $V_{h(l)}$. The initial conditions (the initial values of the flow fields) define the characteristic scales of length $1/k$ and time $1/kV_h$ of the dynamics (5, 6).

Inertial reference frame can be referred to the reference frame moving with a constant velocity $\tilde{\mathbf{V}}_0=(0,0,\tilde{V}_0)$ of a planar interface separating the fluids (5, 11). If, in the laboratory reference frame, the heavy fluid is at rest, then the velocity of planar steady interface is $\tilde{\mathbf{V}}_0=-\mathbf{V}_h$, with $\tilde{\mathbf{V}}_0=(0,0,-V_h)$. Velocity $\tilde{\mathbf{V}}$ of unsteady nonplanar interface obeys relation $\tilde{\mathbf{V}}\cdot\mathbf{n}=-\mathbf{v}\cdot\mathbf{n}|_{\theta=0^+}=-(\tilde{\mathbf{j}}/\rho)\cdot\mathbf{n}\big|_{\theta=0^+}$ (11, 38).

Linearized Dynamics. We define $\theta=-z+z^*(x,t)$, slightly perturb the interface $|\dot{\theta}/|\nabla\theta||<<|\mathbf{V}|$, $|\partial z^*/\partial x|\ll 1$ leading to $\mathbf{n}=\mathbf{n}_0+\mathbf{n}_1$, $\boldsymbol{\tau}=\boldsymbol{\tau}_0+\boldsymbol{\tau}_1$ with $|\mathbf{n}_1|<<|\mathbf{n}_0|$, $|\boldsymbol{\tau}_1|-\ll|\boldsymbol{\tau}_0|$, and slightly perturb the flow fields $\mathbf{v}=\mathbf{V}+\mathbf{u}$, $\tilde{j}=\mathbf{J}+\mathbf{j}$, $P=P_0+p$, $W=W_0+w$ with $|\mathbf{u}|<<|\mathbf{V}|$, $|\mathbf{j}|\ll|\mathbf{J}|$, $|p|<<|P_0|$, $|w|\ll|W_0|$.

To the leading order, $\theta=-z$, $\mathbf{n}=\mathbf{n}_0$, $\boldsymbol{\tau}=\boldsymbol{\tau}_0$ with $\mathbf{n}_0=(0,0,-1)$, $\boldsymbol{\tau}_0=(1,0,0)$. In the bulk, the flow fields are uniform: $(\rho,\mathbf{V},P_0,W_0)=(\rho,\mathbf{V},P_0,W_0)_hH(\theta)+(\rho,\mathbf{V},P_0,W_0)_lH(-\theta)$. With mass flux $\mathbf{J}=\rho\mathbf{V}$ and $J_n=\mathbf{J}\cdot\mathbf{n}_0$, boundary conditions at the interface are

$$[J_n]=0,\quad [(P_0+J_n^2/\rho)\mathbf{n}_0]=0,\quad [J_n((\mathbf{J}\cdot\boldsymbol{\tau}_0)/\rho)\boldsymbol{\tau}_0]=0,\quad [J_n(W_0+\mathbf{J}^2/2\rho^2)\mathbf{n}_0]=0. \qquad [2a]$$

For incompressible dynamics, $[J_n]=0$, $[P_0\ \mathbf{n}_0]=0$, $[J_n((\mathbf{J}\cdot\boldsymbol{\tau}_0)/\rho)\boldsymbol{\tau}_0]=0$, $[J_nW_0]=0$ (5, 6, 40).

To the first order, boundary conditions at the interface are

$$[j_n]=0,\quad [(p+2J_nj_n/\rho)\mathbf{n}_0]=0,\quad [J_n(\mathbf{J}\cdot\boldsymbol{\tau}_1+\mathbf{j}\cdot\boldsymbol{\tau}_0)/\rho]=0,\quad [J_n(w+(\mathbf{J}\cdot\mathbf{j})^2/\rho^2)]=0, \qquad [2b]$$

with $\mathbf{j}=\rho(\mathbf{u}+\mathbf{n}_0\dot{\theta})$, $j_n=\mathbf{j}\cdot\mathbf{n}_0$, $\mathbf{n}_1=(\partial z^*/\partial x,0,0)$, $\boldsymbol{\tau}_1=(0,0,\partial z^*/\partial x)$. For incompressible perturbed dynamics, the enthalpy perturbations are $w_{h(l)}=p_{h(l)}/\rho_{h(l)}$ (5, 20, 40). The governing equations in the bulk and at the outside boundaries are

$$\nabla\cdot\mathbf{u}_{h(l)}=0,\quad \dot{u}_{h(l)}+(\mathbf{V}_{h(l)}\cdot\nabla)\,\mathbf{u}_{h(l)}+\nabla p_{h(l)}/\rho_{h(l)}=0,\quad \mathbf{u}_h|_{z\to-\infty}=0,\quad \mathbf{u}_l|_{z\to+\infty}=0. \qquad [2c]$$

In the laboratory reference frame, the interface velocity $\tilde{\mathbf{V}}$ is $\tilde{\mathbf{V}}=\tilde{\mathbf{V}}_0+\tilde{\mathbf{v}}$, $|\tilde{\mathbf{v}}|\ll|\tilde{\mathbf{V}}_0|$, with $\tilde{\mathbf{V}}\cdot\mathbf{n}_0=-(\tilde{\mathbf{V}}_0+(\mathbf{u}+\dot{\theta}\mathbf{n}_0))\cdot\mathbf{n}_0\big|_{\theta=0^+}$. To the leading order, $\tilde{\mathbf{V}}=\tilde{\mathbf{V}}_0$; the first order perturbation obeys relation $\tilde{\mathbf{v}}\cdot\mathbf{n}_0=-(\mathbf{u}\cdot\mathbf{n}_0+\dot{\theta})\big|_{\theta=0^+}$ (5, 6, 11, 37–40).

Solution Structure. We seek solution such that the velocity of the heavy fluid is potential in accordance with the Kelvin theorem and the velocity of the light fluid can be a superposition of the potential and vortical components (5, 6):

$$\mathbf{u}_h=\nabla\Phi_h,\quad \mathbf{u}_l=\nabla\Phi_l+\nabla\times\boldsymbol{\Psi}_l,\quad z^*=Ze^{ikx+\Omega t}. \qquad [3]$$

Here, $\Phi_h=\Phi e^{ikx+kz+\Omega t}$, $\Phi_l=\tilde{\Phi}e^{ikx-kz+\Omega t}$, $\boldsymbol{\Psi}_l=(0,\Psi_l,0)$, $\Psi_l=\Psi e^{ikx-kz+\Omega t}$, and the growth rate (eigenvalue) is Ω. This yields the vortical field length scale $\tilde{\lambda}=2\pi/\tilde{k}$, $\tilde{k}=\Omega/V_l$ and the pressure perturbations $p_{h(l)}$. In the presence of gravity $\mathbf{g}$ directed from the heavy to the light fluid and with negligible stratification, $p_{h(l)}=-\rho_{h(l)}(\dot{\Phi}_{h(l)}+V_{h(l)}\partial\Phi_{h(l)}/\partial z-gz)$. We use dimensionless values for the growth rate (eigenvalue) $\omega=\Omega/kV_h$, the density ratio $R=\rho_h/\rho_l$ with $R\geq 1$, and the gravity value $G=g/kV_h^2$ with $G\geq 0$. This leads to $V_l/V_h=R$ and $\tilde{k}/k=\omega/R$ (5, 11, 20, 38–40). Scale for pressure perturbations is $\rho_hV_h^2$.

Fundamental Solutions. The governing equations are reduced to a linear system $\mathrm{M}\,\mathbf{r}=0$, where vector $\mathbf{r}=(\Phi_h,\Phi_l,V_hz^*,\Psi_l)^{\mathrm{T}}$ and M is 4×4 matrix. Its elements are functions on ω, R, G. We find eigenvalues ω_i by using condition $\det\mathrm{M}(\omega_i,R,G)=0$ and identify the associated eigenvectors $\mathbf{e}_i$ by reducing matrix $\mathrm{M}=\mathrm{M}(\omega_i,R,G)$ to row-echelon form. The solution $\mathbf{r}$ is a linear combination of fundamental solutions $\mathbf{r}_i=\mathbf{r}_i(\omega_i,\mathbf{e}_i)$ as $\mathbf{r}=\sum_iC_i\mathbf{r}_i$, where C_i are integration constants. In nondegenerate case $i=1,2,3,4$, there are four fundamental solutions for four degrees of freedom (47).

Results—Inertial Dynamics

For inertial dynamics, gravity is zero, $\mathbf{g}=0$, $G=0$.

Conservative Dynamics. Conservative dynamics balances the fluxes of mass, momentum, and energy at the interface. For this dynamics, the matrix M is $\mathrm{M}=M$. Its rank is four. Its determinant is $\det M=i((R-1)^2/R)(\omega-R)(\omega+R)(\omega^2+R)$, and the eigenvalues ω_i and eigenvectors $\mathbf{e}_i$ are

$$\omega_{1(2)}=\pm i\sqrt{R},\mathbf{e}_{1(2)}=(^*,\ ^*,1,0)^{\mathrm{T}};\quad \omega_3=R,\mathbf{e}_3=(0,\ ^*,0,1)^{\mathrm{T}};\quad \omega_4=-R,\mathbf{e}_4=(^*,\ ^*,0,1)^{\mathrm{T}}, \qquad [4]$$

where asterisks mark functions on R (Fig. 1*A*). There are four fundamental solutions. The solutions $\mathbf{r}_{1(2)}(\omega_{1(2)},\mathbf{e}_{1(2)})$ are stable, and their eigenvalues are imaginary: $\omega_2=\omega_1^*$, $\mathbf{e}_2=\mathbf{e}_2^*$. The solution $\mathbf{r}_3(\omega_3,\mathbf{e}_3)$ is unstable, $\mathrm{Re}[\omega_3]>0$, and the solution $\mathbf{r}_4(\omega_4,\mathbf{e}_4)$ is stable, $\mathrm{Re}[\omega_4]<0$.

Fundamental solutions $\mathbf{r}_{1(2)}$ for conservative dynamics describe the flow fields that stably oscillate near the interface and decay away from the interface (20). These solutions are traveling waves. Their interference produces stable standing waves, particularly the solution $\mathbf{r}_{CD}=(\mathbf{r}_1+\mathbf{r}_2)/2$. For solution $\mathbf{r}_{CD}(\omega_{CD},\mathbf{e}_{CD})$, Fig. 2 illustrates the perturbed velocity vector fields $\mathbf{u}_{h(l)}$, the perturbed velocity streamlines $\mathbf{s}_{h(l)}$ defined as $(d\mathbf{s}_{h(l)}/dt)\times\mathbf{u}_{h(l)}=0$, the contour plot of the perturbed pressure $p_{h(l)}$, and the interface perturbation z^* in the (x,z) plane at some density ratio

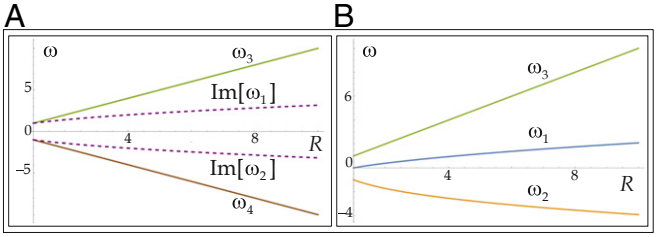

Fig. 1. Dependence of eigenvalues on density ratio. (*A*) Conservative dynamics. (*B*) Classic Landau dynamics.

and some instance of time. Fields of pressure $p_{h(l)}$ are antiphase at the interface, thus causing stable oscillations in the z direction; the extrema of $p_{h(l)}$ correspond to the extrema of z^*; they are symmetric and span the same range of values $\mathrm{R}=(p_{\min},p_{\max})$ with $|p_l|_{\max(min)}/|p_h|_{\max(min)}=1$ and $|\mathrm{R}_l|=|\mathrm{R}_h|$. For solution $\mathbf{r}_{CD}$ [traveling waves $\mathbf{r}_{1(2)}$], the vortical filed and vorticity are zero: $\Psi_l=0$, $\nabla\times\boldsymbol{\Psi}_l=0$, $\nabla\times\mathbf{u}_l=0$ (20).

Fundamental solution $\mathbf{r}_3(\omega_3,\mathbf{e}_3)$, while formally unstable, has zero fields of the perturbed velocity, pressure, and the interface perturbations in the entire domain at any time for any integration constant C_3: $\mathbf{u}_{h(l)}=0$, $p_{h(l)}=0$, $z^*=0$. Fundamental solution $\mathbf{r}_4(\omega_4,\mathbf{e}_4)$ must have the integration constant $C_4=0$ to obey at any time the condition $\mathbf{u}_l|_{z\to+\infty}=0$. This is because its vortical component, $\nabla\times\boldsymbol{\Psi}_l$, increases away from the interface. For solutions $\mathbf{r}_{3(4)}$, the vortical field is $\Psi_l\neq0$, $\nabla\times\boldsymbol{\Psi}_l\neq0$, while the vorticity is $\nabla\times\mathbf{u}_l=0$, with $\nabla\times\mathbf{u}_l=(0,(k^2-\tilde{k}^2)\Psi,0)$ and $(\tilde{k}/k)^2=(\omega/R)^2=1$.

Classic LD Dynamics. Classic Landau dynamics balances the fluxes of mass and normal and tangential components of momentum and uses the continuity of normal component of the perturbed velocity $[\mathbf{u}\cdot\mathbf{n}_0]=0$ at the interface (5, 40). This leads to

$$[j_n]=0,\quad [(p+2J_nj_n/\rho)\,\mathbf{n}_0]=0,\quad [J_n(\mathbf{J}\cdot\boldsymbol{\tau}_1+\mathbf{j}\cdot\boldsymbol{\tau}_0)/\rho]=0,\quad [\mathbf{u}\cdot\mathbf{n}_0]=0. \qquad \textbf{[5a]}$$

For classic Landau system, the matrix M is $\mathrm{M}=L$. Its rank is four. Its determinant is $\det L=i((R-1)/R)(\omega-R)((R+1)\omega^2+2R\omega-(R-1)R)$; the eigenvalues ω_i and eigenvectors $\mathbf{e}_i$ are

$$\omega_{1(2)}=\left(-R\pm\sqrt{(R^3+R^2-R)}\right)\Big/(1+R),\ \mathbf{e}_{1(2)}=(^*,\,^*,\,^*,1)^{\mathrm{T}};\quad \omega_3=R,\ \mathbf{e}_3=(0,\,^*,0,1)^{\mathrm{T}}, \qquad \textbf{[5b]}$$

where asterisks mark functions of R (Fig. 1*B*). There are three fundamental solutions: $i=1,2,3$. Solution $\mathbf{r}_1(\omega_1,\mathbf{e}_1)$ is unstable, $\mathrm{Re}[\omega_1]>0$; solution $\mathbf{r}_2(\omega_2,\mathbf{e}_2)$ is stable; and solution

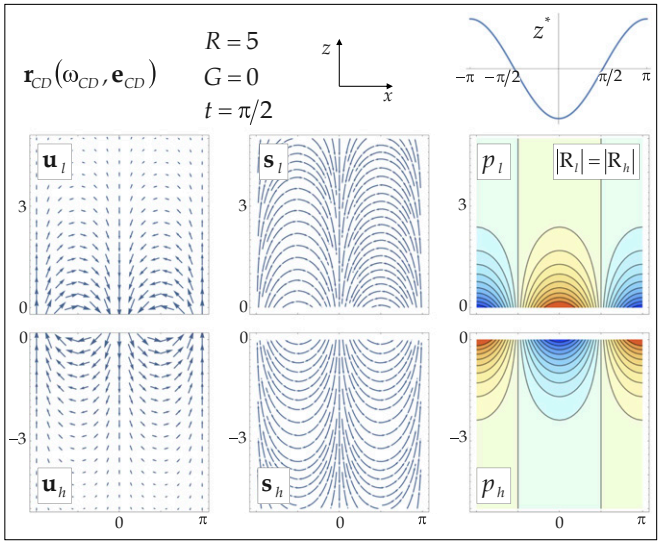

Fig. 2. Flow fields' structure for the inertial conservative dynamics. Plots of real parts of the interface perturbation, the perturbed velocity vector fields, and the perturbed velocity streamlines and the contour plot of the perturbed pressure with red (blue) for positive (negative) values.

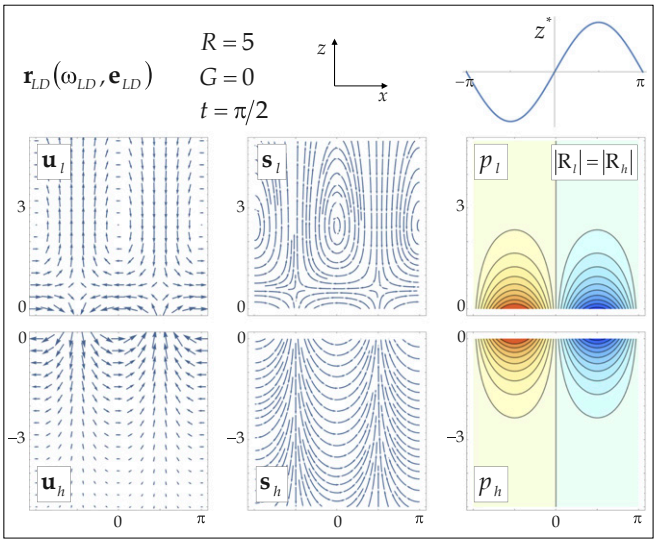

Fig. 3. Flow fields' structure for the classic Landau dynamics. Plots of real parts of the interface perturbation, the perturbed velocity vector fields, and the perturbed velocity streamlines and the contour plot of the perturbed pressure with red (blue) for positive (negative) values.

$\mathbf{r}_3(\omega_3,\mathbf{e}_3)$ is unstable, $\mathrm{Re}[\omega_3]>0$, and is identical to that in the conservative dynamics.

Fundamental solution $\mathbf{r}_1(\omega_1,\mathbf{e}_1)$ for classic Landau system, hereafter $\mathbf{r}_{LD}(\omega_{LD},\mathbf{e}_{LD})$, corresponds to the LDI (5, 40). This solution is a physical solution satisfying the assigned boundary conditions. For solution $\mathbf{r}_{LD}$, the vortical and potential components of the velocities and the interface perturbation are strongly coupled (40). The perturbed velocity fields $\mathbf{u}_{h(l)}$ and the perturbed velocity streamlines $\mathbf{s}_{h(l)}$ illustrate the formation of vortical structures near the interface and in the bulk (Fig. 3). For solution $\mathbf{r}_{LD}$, the vortical component $\nabla\times\boldsymbol{\Psi}_l$ and the vorticity $\nabla\times\mathbf{u}_l$, while increasing in time, as $\sim e^{\omega_{LD}(kV_h)t}$, decay away from the interface, as $\sim e^{-\tilde{k}z}$ (5, 6, 40). The length scale of the vortical field is large, $\tilde{k}/k=\omega_{LD}/R=(-R+\sqrt{-R+R^2+R^3})/R(1+R)$ with $\tilde{k}/k\sim(R-1)/2\to0$ for $R\to1^+$ and $\tilde{k}/k\sim R^{-1/2}\to0$ for $R\to\infty$ (20). The maximum value $\tilde{k}/k$ is achieved at $R=2+\sqrt{5}\approx4.24$. The contribution of the vortical field to the dynamics is significant for fluids with very different densities, $R\to\infty$, and is small for fluids with similar densities, $R\to1^+$. Pressure fields $p_{h(l)}$ are in phase and equal one another at the interface; they are in antiphase with the interface perturbation. Pressure fields $p_{h(l)}$ are symmetric and span the same range of values $\mathrm{R}=(p_{\min},p_{\max})$ with $|p_l|_{\max(min)}/|p_h|_{\max(min)}=1$ and $|\mathrm{R}_l|=|\mathrm{R}_h|$.

For fundamental solution $\mathbf{r}_2(\omega_2,\mathbf{e}_2)$, the interface perturbation, and the vortical and potential components of the velocity field are also coupled. For this solution, we must set the integration constant zero $C_2=0$ to obey at any time the condition $\mathbf{u}_l|_{z\to+\infty}=0$. Fundamental solution $\mathbf{r}_3(\omega_3,\mathbf{e}_3)$ is identical to that in the conservative dynamics and has zero fields for any C_3.

The classic Landau dynamics has a smaller number of fundamental solutions than the degrees of freedom. Eliminating this degeneracy may lead to appearance of a (fourth) neutrally stable solution with a seed vortical field triggering the LDI.

Comparative Study. Conservative dynamics $\mathbf{r}_{CD}(\omega_{CD},\mathbf{e}_{CD})$ and LD dynamics $\mathbf{r}_{LD}(\omega_{LD},\mathbf{e}_{LD})$ have distinct quantitative, qualitative, and formal properties. The dynamics $\mathbf{r}_{CD}$ is stable, and the dynamics $\mathbf{r}_{LD}$ is unstable. For $\mathbf{r}_{CD}$, the velocity fields are potential; for $\mathbf{r}_{LD}$, the potential and vortical velocity components are strongly

coupled. Solution $\mathbf{r}_{CD}$ conserves mass, momentum, and energy at the interface; solution $\mathbf{r}_{LDG}$ conserves mass and momentum and has zero perturbed mass flux at the interface. The conservative dynamics is nondegenerate; the LD dynamics is degenerate (Figs. 1 and 3).

Mechanisms of Stabilization and Destabilization. To better understand the mechanism(s) of the interface (de-)stabilization, we consider the interface velocity (11, 38–40). In the laboratory reference frame, the interface velocity is $\tilde{\mathbf{V}}=\tilde{\mathbf{V}}_0+\tilde{\mathbf{v}}$, with $\tilde{\mathbf{v}}\cdot\mathbf{n}_0=-(\mathbf{u}\cdot\mathbf{n}_0+\dot{\theta})\big|_{\theta=0^+}$. For dynamics $\mathbf{r}_{CD}$, the values are $\mathbf{u}\cdot\mathbf{n}_0|_{\theta=0^+}\sim e^{\pm i\sqrt{R}t}$, $\dot{\theta}\big|_{\theta=0^+}\sim e^{\pm i\sqrt{R}t}$, leading to $(\mathbf{u}\cdot\mathbf{n}_0+\dot{\theta})\big|_{\theta=0^+}\sim e^{\pm i\sqrt{R}t}$ and $\tilde{v}\cdot\mathbf{n}_0\sim e^{\pm i\sqrt{R}t}$. Thus, the interface velocity experiences small stable oscillations near the steady value $\tilde{\mathbf{V}}_0$, $(\tilde{\mathbf{V}}-\tilde{\mathbf{V}}_0)\cdot\mathbf{n}_0\sim e^{\pm i\sqrt{R}\,t}$.

This suggests the inertial effect as the stabilization mechanism of the conservative dynamics $\mathbf{r}_{CD}$. Indeed, when the interface is slightly perturbed, the parcels of the heavy fluid and the light fluid follow the interface perturbation, causing the change of momentum and energy of the fluid system. However, the dynamics is inertial. To conserve the momentum and energy, the interface as a whole slightly changes its velocity. Thus, the reactive force occurs and stabilizes the dynamics.

For the LD dynamics $\mathbf{r}_{LD}$, the interface velocity is constant, $\tilde{\mathbf{V}}=\tilde{\mathbf{V}}_0$, as it is postulated in the boundary condition $[\mathbf{u}\cdot\mathbf{n}_0]=0$, leading to $(\mathbf{u}\cdot\mathbf{n}_0+\dot{\theta})\big|_{\theta=0^+}=0$, $\tilde{\mathbf{V}}=0$ (5, 40). Since in classic LD dynamics, mass and momentum are conserved, for capturing the destabilization mechanism, we consider how the condition $[\mathbf{u}\cdot\mathbf{n}_0]=0$ may influence the energy transport.

Remarkably, for ideal incompressible fluids, the solution $\mathbf{r}_{LD}$ is incompatible with the condition for energy balance at the perturbed interface (20). Indeed, by substituting $[\mathbf{u}\cdot\mathbf{n}]=0$ ($j_n=0$) in the condition for energy balance $[J_n(w+(\mathbf{J}\cdot\mathbf{j})/\rho^2)]=0$, one obtains $[J_n(w+(\mathbf{J}\cdot\mathbf{j})/\rho^2)]=[J_n w]=0$ and with $[J_n]=0$, reduces it further to $[w]=0$ (20).

The enthalpy perturbations are $w=p/\rho+\delta e$, where δe are the fluctuations of internal energy (in physics sense) (5, 20). In ideal incompressible fluids, free of energy sources, these fluctuations are zero, $\delta e=0$, because $\dot{e}=0$, $\nabla e=0$. Thus, with $w=p/\rho$ and with $\rho_h\neq\rho_l$, the condition for energy balance, $[w]=0$, contradicts the condition for momentum balance, $[p]=0$. We see that, for ideal incompressible fluids, classic Landau dynamics, while conserving enthalpy (in physics sense) to the leading order, $[W_0]=0$, requires energy imbalance at the interface to the first order. This imbalance is induced by the first-order enthalpy perturbations, $[w]=[p/\rho]$. This is the work done by the fluid when a parcel of fluid of a unit mass expands its volume from ρ_h^{-1} to ρ_l^{-1} under pressure p.

In realistic fluids, this energy imbalance can be induced by energy fluctuations. The effect can be self-consistently derived from entropy conditions with account for chemical reactions. In ideal fluids, to quantify the effect of energy imbalance on the interface stability, we can introduce an additional artificial energy flux; study a transition from stable to unstable dynamics with increase of the fluctuations' strength; and find that, for strong (weak) fluctuations, the eigenvalues and the flow fields are similar to those in the classic Landau (conservative) dynamics (20) (*SI Appendix*).

Chemistry-Induced Instabilities. In reactive fluids, it is generally well-understood that chemically reactive systems can be hydrodynamically unstable. However, it is a challenge to construct a model experiment or a simulation that cleanly displays significant chemical reaction instability at a simple interface. The paper in ref. 46 reports atomistic simulations for studying the energy transport in a reactive system and the effect of chemical reaction on the interface stability. Additional investigations are required to fully understand the properties of chemistry-induced instabilities at atomistic and continuous scales.

Results—Accelerated Dynamics

For accelerated dynamics, gravity $\mathbf{g}$ is directed from the heavy to the light fluid, $G>0$.

Accelerated Conservative Dynamics. For conservative dynamics balancing the mass, momentum, and energy at the interface, matrix M is $\mathrm{M}=M_G$, its determinant is $\det M_G=i((R-1)^2/R)(\omega-R)(\omega+R)(\omega^2+R(1-G/G_{cr}))$, and the eigenvalues ω_i and eigenvectors $\mathbf{e}_i$ are

$$\omega_{1(2)}=\pm i\sqrt{R}\sqrt{1-G/G_{cr}},\mathbf{e}_{1(2)}=(*,*,1,0)^{\mathrm{T}};\quad \omega_3=R,\mathbf{e}_3=(0,*,0,1)^{\mathrm{T}};\quad \omega_4=-R,\mathbf{e}_4=(*,*,0,1)^{\mathrm{T}}, \qquad [6]$$

where $G_{cr}=R(R-1)/(R+1)$ and asterisks mark functions of R, G (Fig. 4*A*).

Solutions $\mathbf{r}_1(\omega_1,\mathbf{e}_1)$ and $\mathbf{r}_2(\omega_2,\mathbf{e}_2)$ depend on the value G. For $G<G_{cr}$, the eigenvalues are imaginary, and the solutions $\mathbf{r}_{1(2)}$ are stable, $\omega_2=\omega_1^*$, $\mathbf{e}_2=\mathbf{e}_2^*$. Solutions $\mathbf{r}_{1(2)}$ are traveling waves; their interference results in the appearance of stable standing waves. For $G>G_{cr}$, $\omega_1=\sqrt{R}\sqrt{G/G_{cr}-1}$, and $\mathrm{Re}[\omega_1]>0$, fundamental solution $\mathbf{r}_1(\omega_1,\mathbf{e}_1)$, hereafter $\mathbf{r}_{CDG}(\omega_{CDG},\mathbf{e}_{CDG})$, is unstable and describes exponential growth of the interface perturbations. For $G>G_{cr}$, $\omega_2=-\sqrt{R}\sqrt{G/G_{cr}-1}$, and $\mathrm{Re}[\omega_2]<0$, solution $\mathbf{r}_2$ is stable and describes exponential decay of the perturbations. The critical value $G_{cr}=R(R-1)/(R+1)$ approaches $G_{cr}\to R$ for $R\to\infty$ and $G_{cr}\to(R-1)/2$ for $R\to 1^+$. Solutions $\mathbf{r}_{3(4)}(\omega_{3(4)},\mathbf{e}_{3(4)})$ do not depend on the value of G and are the same as the corresponding solutions in the inertial dynamics. Solution $\mathbf{r}_3$ is unstable, $\mathrm{Re}[\omega_3]>0$, and solution $\mathbf{r}_4$ is stable, $\mathrm{Re}[\omega_4]<0$.

For accelerated conservative dynamics $\mathbf{r}_{CDG}(\omega_{CDG},\mathbf{e}_{CDG})$, the velocity fields are potential in the stable, $G<G_{cr}$, and unstable, $G>G_{cr}$, regimes. For this solution, the transports of mass, momentum, and energy are balanced at the interface, the conditions at the outside boundaries are obeyed, and the vortical field and vorticity are zero, $\Psi_l=0$, $\nabla\times\boldsymbol{\Psi}_l=0$, $\nabla\times\mathbf{u}_l=0$. In the stable regime $G<G_{cr}$, the fields of velocity, stream lines, and pressure of solution $\mathbf{r}_{CDG}$ have features similar to those of the inertial dynamics $\mathbf{r}_{CD}$. In the unstable regime, $G>G_{cr}$, the fields of pressure $p_{h(l)}$ are in phase with one another and with the interface perturbation. However, they are no longer symmetric; their values differ significantly and span distinct range $\mathrm{R}=(p_{\min},p_{\max})$ with $|p_l|_{\max(min)}/|p_h|_{\max(min)}\ll 1$ and $|\mathrm{R}_l|\ll|\mathrm{R}_h|$. This illustrates the formation of a periodic (finger-type) structure of bubbles and spikes, with a bubble (spike) being a portion of the heavy (light) fluid penetrating the light (heavy) fluid (Fig. 5).

For solution $\mathbf{r}_2$, the velocity fields are qualitatively similar to those for $\mathbf{r}_{CDG}$. For solution $\mathbf{r}_3$, the fields of velocity, pressure, and interface perturbation are zero for any constant C_3; for solution $\mathbf{r}_4$, the integration constant must be zero $C_4=0$ to obey conditions at the domain boundaries.

Accelerated LD Dynamics. For accelerated LDI, the dynamics balances the fluxes of mass, normal and tangential components of momentum, and the normal component of the perturbed velocity $[\mathbf{u}\cdot\mathbf{n}_0]=0$ (5, 6). This leads to matrix $\mathrm{M}=L_G$ with

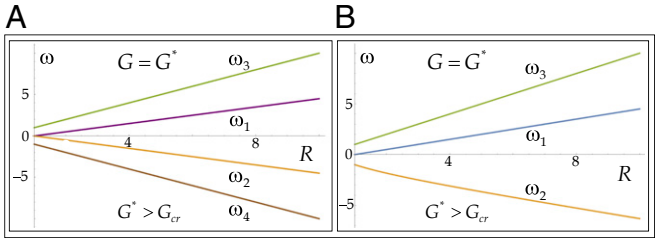

Fig. 4. Dependence of eigenvalues on density ratio at some gravity value. (*A*) Accelerated conservative dynamics. (*B*) Accelerated Landau dynamics.

det $L_G = i((R-1)/R)(\omega - R)((R+1)\omega^2 + 2R\omega - (R-1)(R+G))$; the eigenvalues ω_i and eigenvectors $\mathbf{e}_i$ are

$$\omega_{1(2)} = \left(-R \pm \sqrt{(R^3+R^2-R)+G(R^2-1)}\right)\Big/(1+R), \quad \mathbf{e}_{1(2)} = (*,*,*,1)^{\mathrm{T}}; \quad \omega_3 = R, \mathbf{e}_3 = (0,*,0,1)^{\mathrm{T}}, \qquad [7]$$

where asterisks mark functions of R, G (Fig. 4*B*). Solutions $\mathbf{r}_{1(2)}(\omega_{1(2)}, \mathbf{e}_{1(2)})$ depend on G. Solution $\mathbf{r}_3(\omega_3, \mathbf{e}_3)$ is independent of G and is identical to that in the inertial dynamics.

Fundamental solution $\mathbf{r}_1(\omega_1, \mathbf{e}_1)$, hereafter $\mathbf{r}_{LDG}(\omega_{LDG}, \mathbf{e}_{LDG})$, corresponds to the LDI in gravity field (Fig. 6). It is unstable for any $G > 0$ (5, 6). For solution $\mathbf{r}_{LDG}$, the transports of mass, momentum, and perturbed mass flux are balanced at the interface; the conditions at the outside boundaries are obeyed, the potential and vortical components of the velocities and the interface perturbation are coupled, and the vortical field length scale is $\tilde{k} = k(-R + \sqrt{(R^3+R^2-R)+G(R^2-1)})/(R(1+R))$. For large G, the pressure fields $p_{h(l)}$ are not symmetric and span a significantly distinct range of values $\mathrm{R} = (p_{\min}, p_{\max})$ with $|p_l|_{\max(min)}/|p_h|_{\max(min)} << 1$ and $|\mathrm{R}_l| \ll |\mathrm{R}_h|$. They are in phase with one another and with the interface perturbation z^*.

For solution $\mathbf{r}_2$, the interface perturbation and the vortical and potential components of velocities are also coupled. For this solution, we must set the constant $C_2 = 0$ to obey at any time the condition $\mathbf{u}_l|_{z\to+\infty} = 0$. Solution $\mathbf{r}_3$ has zero fields in the entire domain at any time for any C_3 as in the inertial dynamics.

Accelerated RT Dynamics. For the RTI (22, 23), there is no mass flux at the interface, and there is no fluid motion far from the interface. This leads to the boundary conditions

$$\left[\tilde{j}_n\right] = 0, \quad [P\mathbf{n}] = 0, \quad [\mathbf{v}\cdot\mathbf{n}] = 0, \quad \mathbf{v}_h|_{z\to-\infty} = (0,0,0), \quad \mathbf{v}_l|_{z\to+\infty} = (0,0,0), \qquad [8a]$$

with $[\mathbf{v}\cdot\boldsymbol{\tau}] = any$, $[W] = any$ (5). We slightly perturb the interface $\theta = -z + z^*(x,t)$, $z^* = Ze^{ikx+\Omega t}$, with $|\dot{\theta}/|\nabla\theta|| << \sqrt{g/k}$, $|\partial z^*/\partial x| \ll 1$. We slightly perturb the velocities with potential fields $\mathbf{v}_h = \nabla\Phi_h$, $\Phi_h = \Phi e^{ikx+kz+\Omega t}$ and $\mathbf{v}_l = \nabla\Phi_l$, $\Phi_l = \tilde{\Phi}e^{ikx-kz+\Omega t}$, with $|\mathbf{v}| \ll \sqrt{g/k}$ and perturb the fluid pressure $P = P_0 + p$, $|p| \ll |P_0|$, with $p_{h(l)} = -\rho_{h(l)}(\dot{\Phi}_{h(l)} + V_{h(l)}\partial\Phi_{h(l)}/\partial z - gz)$. The governing equations are reduced to a linear system $\mathrm{M}\,\mathbf{r} = 0$, where vector is $\mathbf{r} = (\Phi_h, \Phi_l, V_h z^*)^{\mathrm{T}}$ and the 3 × 3 matrix is $\mathrm{M} = \mathrm{M}(\omega, R, G)$. The solution is $\mathbf{r} = \sum_i C_i\mathbf{r}_i$, where $\mathbf{r}_i = \mathbf{r}_i(\omega_i, \mathbf{e}_i)$ are fundamental solutions, C_i are constants, and $i = 1,2,3$ in the nondegenerate case (47). For RT dynamics, matrix M is $\mathrm{M} = T_G$. Its determinant is $\det T_G = (R-1)((R+1)\omega^2 - G(R-1))$, and ω_i and $\mathbf{e}_i$ are

$$\omega_{1(2)} = \pm\sqrt{G(R-1)/(R+1)}, \quad \mathbf{e}_{1(2)} = (*,*,1)^{\mathrm{T}}, \qquad [8b]$$

where asterisks mark functions of R, G. Note that, while in RTI, the length scale and timescale are $1/k$ and $1/\sqrt{gk}$, to conduct a comparative study, we scale the time with $1/kV_h$, where V_h is now understood as some velocity scale, leading to $g = G\,(kV_h^2)$ as before.

For any $G > 0$, fundamental solution $\mathbf{r}_1(\omega_1, \mathbf{e}_1)$, hereafter $\mathbf{r}_{RT}(\omega_{RT}, \mathbf{e}_{RT})$, is unstable and corresponds to the RTI. Its velocity fields are potential, $\nabla\times\mathbf{v}_{h(l)} = 0$, and have shear at the interface. Fundamental solution $\mathbf{r}_2(\omega_2, \mathbf{e}_2)$ is stable and has potential velocity fields. The RT dynamics is degenerate (two fundamental solutions, three degrees of freedom). Eliminating this degeneracy can produce a neutrally stable solution with a "seed" velocity shear at the fluid interface.

Comparative Study. While large gravity values destabilize the interface, the accelerated conservative dynamics $\mathbf{r}_{CDG}(\omega_{CDG}, \mathbf{e}_{CDG})$, the accelerated LD dynamics $\mathbf{r}_{LDG}(\omega_{LDG}, \mathbf{e}_{LDG})$, and the RT dynamics $\mathbf{r}_{RT}(\omega_{RT}, \mathbf{e}_{RT})$ have distinct quantitative, qualitative, and formal properties.

For solution $\mathbf{r}_{CDG}$, the instability develops only when the gravity value exceeds a threshold, $G > G_{cr}$, whereas for solutions $\mathbf{r}_{LDG}$ and $\mathbf{r}_{RT}$, the dynamics is unstable for any $G > 0$. For $G \to 0$, the dynamics $\mathbf{r}_{CDG}$ is stable, $\omega_{CDG} \to i\sqrt{R}$; the dynamics $\mathbf{r}_{RT}$ is neutrally stable, $\omega_{RT} \to 0$; and the dynamics $\mathbf{r}_{LDG}$ is unstable, $\omega_{LDG} \to (-R + \sqrt{R^3+R^2-R})/(1+R)$. For $G \to \infty$, the dynamics $\mathbf{r}_{CDG}$, $\mathbf{r}_{LDG}$, $\mathbf{r}_{RT}$ is unstable, and growth rates are $\omega_{CDG} \to \sqrt{RG/G_{cr}}$, $\omega_{RT} = \sqrt{G(R-1)/(R+1)}$, $\omega_{LDG} \to \omega_{RT}$. There exists a special gravity value of $G = G^*$ at which all of the growth rates are equal: $\omega_{CDG} = \omega_{LDG} = \omega_{RT}$. This is $G^* = (R^2-1)/4$, $G^* > G_{cr}$. Solution $\mathbf{r}_{CDG}$ has the smallest growth rate for $G_{cr} < G < G^*$, $\omega_{CDG} < \omega_{RT} < \omega_{LDG}$, and the largest growth rate for $G > G^*$, $\omega_{CDG} > \omega_{RT} > \omega_{LDG}$. For $G \to \infty$, the accelerated conservative dynamics has the largest growth rate, with $\omega_{CDG}/\omega_{RT(LDG)} \to (R+1)/(R-1)$ (Fig. 7).

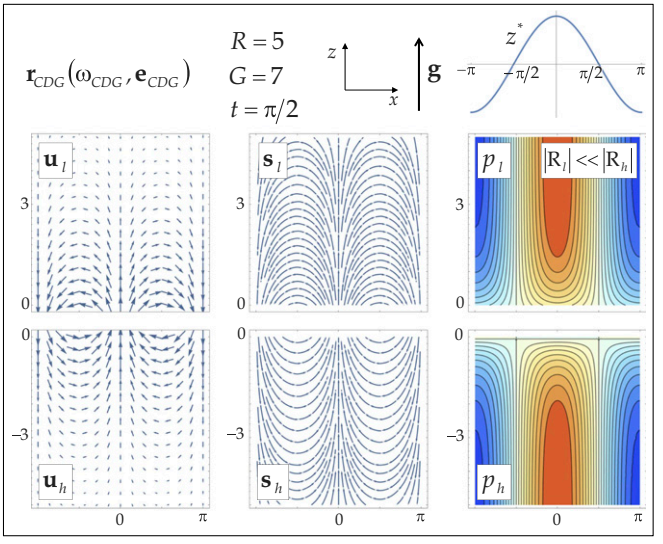

Fig. 5. Flow fields' structure for the accelerated conservative dynamics. Plots of real parts of the interface perturbation, the perturbed velocity vector fields, and the perturbed velocity streamlines and the contour plot of perturbed pressure with red (blue) for positive (negative) values.

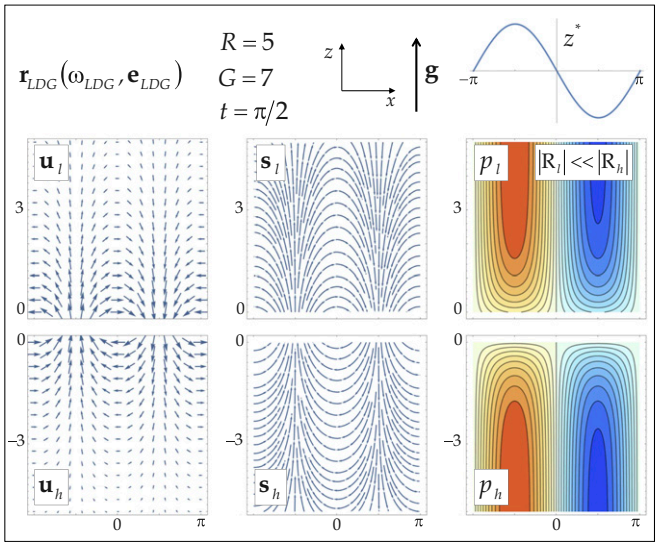

Fig. 6. Flow fields' structure for the accelerated Landau dynamics. Plots of real parts of the interface perturbation, the perturbed velocity vector fields, and the perturbed velocity streamlines and the contour plot of perturbed pressure with red (blue) for positive (negative) values.

Solutions $\mathbf{r}_{CDG}$, $\mathbf{r}_{LDG}$, $\mathbf{r}_{RT}$ have distinct flow fields in the bulk and at the interface. In the bulk, solutions $\mathbf{r}_{CDG}$, $\mathbf{r}_{RT}$ have potential velocity fields, whereas for solution $\mathbf{r}_{LDG}$, the potential and vortical components of the velocity fields are strongly coupled. Solutions $\mathbf{r}_{CDG}$, $\mathbf{r}_{LDG}$ are shear-free at the interface, whereas solution $\mathbf{r}_{RT}$ has the interfacial shear leading to the development of Kelvin–Helmholtz instability and the interfacial vortical structures (22–31).

Solutions $\mathbf{r}_{CDG}$, $\mathbf{r}_{LDG}$, $\mathbf{r}_{RT}$ have distinct physical and formal properties. At the interface, solution $\mathbf{r}_{CDG}$ conserves mass, momentum, and energy; solution $\mathbf{r}_{LDG}$ conserves mass, momentum, and perturbed mass flux; and solution $\mathbf{r}_{RT}$ conserves mass and normal component of momentum. Conservative dynamics is nondegenerate, the LD dynamics is degenerate, and the RT dynamics is degenerate. The degeneracy indicates a singular and ill-posed character of the LDI and the RTI (2, 3).

Mechanisms of Stabilization and Destabilization. The stabilization mechanism of the accelerated conservative dynamics is revealed by the qualitative dependence of the solution $\mathbf{r}_{CDG}$ on the gravity value. At vanishing gravity $G \to 0$, the accelerated dynamics becomes inertial, $\mathbf{r}_{CDG} \to \mathbf{r}_{CD}$, and stable, $\omega_{CDG} \to \omega_{CD}$, with $\omega_{CD} = i\sqrt{R}$. The dynamics is stabilized by the inertial effects. For small gravity values, $G < G_{cr}$, the inertial effects dominate, and the conservative dynamics is stable. For large gravity values, $G > G_{cr}$, the buoyancy effects dominate and destabilize the conservative dynamics.

While velocity fields in accelerated conservative dynamics $\mathbf{r}_{CDG}$ are potential in the bulk, this instability is distinct from the RTI. For any gravity value, $G > 0$, the RT dynamics has no fluid motion away from the interface; it has zero mass flux and has shear at the interface; it is neutrally stable $\omega_{RT} \to 0$ for $G \to 0$. In accelerated conservative dynamics $\mathbf{r}_{CDG}$, there are mass flux across the interface, uniform motions of the fluids far from the interface, and zero shear at the interface; yet, this instability is distinct from the LDI. The LDI has vortical fields; it is unstable $\omega_{LDG} \to \omega_{LD}$ for $G \to 0$.

These results are consistent with the dependence of the interface velocity on the gravity value. In the laboratory reference frame, the interface velocity is $\tilde{\mathbf{V}} = \tilde{\mathbf{V}}_0 + \tilde{\mathbf{v}}$, $\tilde{\mathbf{v}} \cdot \mathbf{n}_0 = -(\mathbf{u}_h \mathbf{n}_0 + \dot{\theta})\big|_{\theta=0^+}$. For accelerated conservative dynamics $\mathbf{r}_{CDG}$, in the stable regime, $G \in [0, G_{cr})$, the interface velocity experiences stable oscillations near the steady value $\tilde{\mathbf{V}}_0$ with $(\tilde{\mathbf{V}} - \tilde{V}_0) \cdot \mathbf{n}_0 = (\mathbf{u}_h \mathbf{n}_0 + \dot{\theta})\big|_{\theta=0^+} \sim e^{i|\omega_{CDG}|t}$. In the unstable regime, $G > G_{cr}$, the velocity of the interface as a whole increases with time. In the linear regime, this increase is exponential, $(\mathbf{u}_h \mathbf{n}_0 + \dot{\theta})\big|_{\theta=0^+} \sim e^{\omega_{CDG} t}$. In the advanced stages, we may expect it to be a power law function of time (2, 3). For RT dynamics $\mathbf{r}_{RT}$, the velocity of the interface as a whole is zero in the linear regime and is a power law function of time, $\sim gt^2$, in the advanced mixing regime (2, 3, 26, 30). For the accelerated LD dynamics $\mathbf{r}_{LDG}$, the interface velocity is constant, $\tilde{\mathbf{V}} = \tilde{\mathbf{V}}_0$ (5, 6).

For large accelerations, $G > G^*$, the unstable dynamics $\mathbf{r}_{CDG(LDG,\,RT)}$ transforms the interface to a periodic structure of bubbles and spikes: The heavy (light) fluid is pushed into the light (heavy) fluid in spikes (bubbles) by the difference of the higher pressure in the heavy (light) fluid and the lower pressure in the light (heavy) fluid. The counterflows develop with fingers of "heavy spikes" and "light bubbles," in agreement with observations (Figs. 5 and 6) (2, 3, 26, 30).

In dimensional units, for given values V_h, g, ρ_h, ρ_l for the accelerated conservative dynamics, we further find the critical wave vector $k_{cr} = (g/V_h^2)(\rho_l/\rho_h)(\rho_h + \rho_l)/(\rho_h - \rho_l)$ at which the interface is stabilized, $\Omega_{CDG}|_{k=k_{cr}} = 0$, and the maximum wave vector $k_{\max} = k_{cr}/2$ at which the unstable interface has the fastest growth, $\partial\Omega_{CDG}/\partial k|_{k=k_{\max}} = 0$, $\partial^2\Omega_{CDG}/\partial k^2\big|_{k=k_{\max}} < 0$.

Effect of Surface Tension. Our general framework enables the systematic study of interfacial dynamics influenced by surface tension, thermal conductivity, compressibility, viscosity, mass ablation, and flow geometry and dimensionality, upon the corresponding modification of the governing equations. Here we briefly consider the effect of surface tension. It is important in multiphase flows, and is straightforward to account for. The outline of results is given in the *SI Appendix*. Note that stabilizations of the conservative dynamics by the inertial effect and by the surface tension are distinct mechanisms.

Discussion

Interfacial mixing is a nonequilibrium process coupling kinetic to macroscopic scales (1). Grasping fundamentals of the interfacial dynamics is crucial for science, mathematics, and engineering (2–6). This work is focused on the classic problem of stability of a fluid interface (phase boundary) that has a mass flux across it (5, 6, 40).

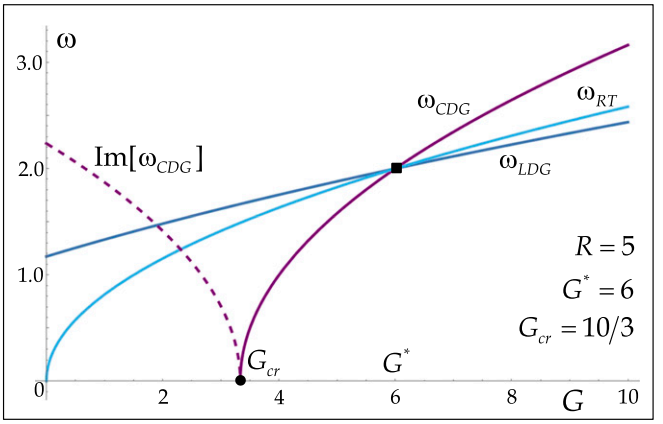

Fig. 7. Dependence of the growth rates of the instabilities on gravity value.

We have briefly reviewed the recent advances in theoretical and experimental studies, have developed the general theoretical framework to systematically study the interface stability and the flow fields, and have identified the mechanisms of interface stabilization and destabilization in the inertial and accelerated flows that have not been discussed in earlier studies (5, 6, 32–45) (Figs. 1–7).

Our theoretical framework is consistent with and generalizes the classic approach (5, 40); directly links the flow fields to the boundary conditions at the interface; and assumes sharp changes of the flow quantities at the interface and negligible effects of dissipation, diffusion, compressibility, and interface thickness. By examining the interface from a far field in a sample case of a 2D flow, we found extreme sensitivity of the dynamics to the interfacial boundary conditions and discovered properties that have not been identified before (Figs. 1–7).

The inertial conservative dynamics is stable and is stabilized by the reactive force. The flow is a superposition of two motions—the background motion of the fluids following the interface with slightly oscillating velocity and stable oscillations of the interface perturbations (Figs. 1–3). For classic Landau dynamics, the interface velocity is constant, the reactive force is absent, and the dynamics is unstable. An energy imbalance may enable the LDI to occur. In reactive fluids, the energy imbalance can be due to chemical reactions (46). The LD unstable dynamics is a superposition of two motions—the background motion of the fluids following the interface with the constant velocity and the growth of the interface perturbations (Figs. 1–3).

For accelerated conservative dynamics, the flow stability depends on the interplay of inertia and buoyancy (i.e., reactive force and gravity) (Figs. 4–7). For gravity values smaller than a threshold, the dynamics is stabilized by inertial effect and reactive force. For large gravity values, buoyancy effect dominates, and gravity destabilizes the flow. The dynamics is a superposition of two motions. Below the threshold, these are the background motion of the fluids following the interface with slightly oscillating velocity and stable oscillations of the interface perturbations. Above the threshold, the interface perturbations grow and therefore, it is the interface velocity. For strong accelerations, this instability grows faster than the accelerated LDI and RTI; for weak acceleration, the LDI has the largest growth rate.

For unstable conservative dynamics in a gravity field, the flow is potential in the fluids' bulk, similar to the RTI and in contrast to the accelerated LDI; it is shear-free at the interface, similar to the LDI and in contrast to the RTI. The conservative dynamics is nondegenerate in contrast to the LDI and the RTI. The degeneracy suggests a singular (ill-posed) character of the RT and LD dynamics requiring the (neutrally stable) seed vortical field in the bulk for the LDI or the seed interfacial shear for the RTI.

It is commonly believed that an interface separating nearly ideal incompressible fluids and having an interfacial mass flux is subject to the LDI at large scales and that, in realistic environment, the LDI is a challenge to implement, because the effects of dissipation, diffusion, and finite interface thickness stabilize the small scales (5, 6, 11, 12, 37–39). Our far-field analysis is fully consistent with these results: For fluids with similar densities, $R \sim O(1)$, the contribution of vortical fields to the dynamics is small, and the fluxes induced in realistic fluids by the stabilizing effects may dominate the dynamics and define the interface stability (5, 6, 11, 20, 37–39, 44, 45). For fluids with very different densities, $R >> 1$, a more careful consideration is required (2–4, 20). Our analysis yields the qualitative and quantitative characteristics of the dynamics that have not been measured before and that can be diagnosed (20, 46) (Eqs. **1**–**8**, Figs. 1–7, and *SI Appendix*).

One such experiment can be a study of the dynamics of fluids with very different densities, with diagnostics of the flow fields near the interface and in the fluids' bulk, and with the measurements of the interface evolution, including the interface velocity as a whole and the interface perturbation growth rate. By comparing the observations with our benchmarks, one can further identify the fundamentals of the interfacial dynamics in realistic environments and elaborate approaches for the flow control (Figs. 1–7) (1–3, 20).

Several questions may frame these perspective studies (20, 46). Can the LDI unconditionally develop at the large scales (20) (Eqs. **4** and **5** and Figs. 1–3)? How can the dynamics be stabilized—by inertial effect, by dissipation and diffusion, or by their combination? How strong should energy fluctuations be to destabilize the flow (20) (*SI Appendix*)? Can these fluctuations be induced by chemical reactions (46)? If so, how are the properties of chemistry-induced instabilities compared with those of the LDI (46)?

For accelerated dynamics, our results suggest that the conservative dynamics is driven by the interplay of the effects of inertia and buoyancy (reactive force and gravity). These results are consistent with recent studies of ablative Rayleigh–Taylor and Richtmyer–Meshkov (RMI) instabilities in compressible fluids (32–35, 41–43). Our analysis yields the properties of the accelerated interfacial dynamics that have not been discussed before (Eq. **6** and Figs. 4–7).

According to our results, the conservative dynamics can be stable even for ideal incompressible fluids at any density ratio when the gravity value is smaller than a threshold (Fig. 7). In the stable regime, the interface velocity experiences stable oscillations, whereas in the unstable regime, along with the growth of interface perturbations, the interface velocity may also increase. The latter qualitatively explains the intensive material mixing observed in experiments in inertial confinement fusion (7, 33, 35). Thus, our analysis can self-consistently resolve this long-standing puzzle. Note that our conservative dynamics instability is the fastest (compared with the LDI and the RTI) in the extreme regime of strong accelerations that are common in high-energy density plasmas (32–34).

For our accelerated conservative dynamics with the growth rate $\Omega_{CDG} = kV_h\sqrt{(\rho_h/\rho_l)(g/g_{cr}-1)}$, experiments and simulations can be conducted on the basis of our results. For given g, V_h, (ρ_h/ρ_l), by varying k, one may observe the interface stabilization at k_{cr} and the fastest instability growth at $k_{\max} = k_{cr}/2$. For given V_h, (ρ_h/ρ_l), k, by varying gravity g, one may observe stable oscillations of the interface with $\Omega_{CDG} = ikV_h\sqrt{\rho_h/\rho_l}$ for $g \ll g_{cr}$ and unstable growth of the perturbations with $\Omega_{CDG} = kV_h\sqrt{(\rho_h/\rho_l)g/g_{cr}}$ for $g >> g_{cr}$. For given g, (ρ_h/ρ_l), k, by varying V_h, one may observe stable oscillations for large V_h and unstable perturbation growth for small V_h.

Existing experimental and numerical studies of the interface stability are focused on the growth of the perturbation amplitude (5–7, 11, 33–39). Our analysis derives the amplitude growth rate and finds that the dynamics is highly sensitive to interfacial boundary conditions. According to our theory, by measuring at macroscopic scales the flow fields in the bulk and at the interface, one can capture the transport properties at microscopic scales at the interface (Figs. 1–7). This information is especially important for systems where experimental data are a challenge to obtain (7, 8, 13, 15, 16, 32–39).

Our approach can systematically incorporate the effects of dissipation, diffusion, compressibility, radiation transport, stratification, finite interface thickness, and nonlocal forces that are important for material dynamics in realistic environments (5, 7–16). According to our results, at small length scales, the interface dynamics can be stabilized by surface tension that influences critical (maximum) wave

vector k_{cr} (k_{max}) for given values of $g, V_h, \sigma, \rho_h, \rho_h/\rho_l$. Our approach can be applied to analyze the interplay of interface stability with structure of flow fields at various experimental parameters. It substantiates perspectives of development of a unified theoretical framework for studies of interfacial dynamics in a broad range of phenomena, including D'yakov–Kontorovich instability in shocks (48, 49), ablative RTI and RMI in fusion plasmas (7, 32–35), deflagration-to-detonation transition in supernova (8, 9, 36), and dynamics of reactive and supercritical fluids (6, 20, 37, 46).

Acknowledgments

We thank the University of Western Australia, the National Science Foundation, and the Summer Undergraduate Research Fellowship Program at the California Institute of Technology.

1 Abarzhi SI, Gauthier S, Sreenivasan KR (2013) Turbulent mixing and beyond: Non-equilibrium processes from atomistic to astrophysical scales. *Philos Trans A Math Phys Eng Sci* 371:20130268.
2 Abarzhi SI (2010) Review of theoretical modelling approaches of Rayleigh-Taylor instabilities and turbulent mixing. *Philos Trans A Math Phys Eng Sci* 368:1809–1828.
3 Anisimov SI, Drake RP, Gauthier S, Meshkov EE, Abarzhi SI (2013) What is certain and what is not so certain in our knowledge of Rayleigh-Taylor mixing? *Philos Trans A Math Phys Eng Sci* 371:20130266.
4 Mayo SL, Olafson BD, Goddard WA (1990) DREIDING: A generic force field for molecular simulations. *J Phys Chem* 9:8897–8909.
5 Landau LD, Lifshitz EM (1987) *Course of Theoretical Physics I–IX* (Pergamon, New York).
6 Zeldovich YB (1985) *The Mathematical Theory of Combustion and Explosions* (Springer, Berlin).
7 Haan SW, et al. (2011) Point design targets, specifications, and requirements for 2010 ignition campaign on NIF. *Phys Plasmas* 18:051001.
8 Arnett D (1996) *Supernovae and Nucleosynthesis* (Princeton Univ Press, Princeton).
9 Arnett WD, Meakin C, Young PA (2009) Turbulent convection in stellar interiors. II. The velocity field. *Astrophys J* 690:1715–1729.
10 Mahalov A (2014) Multiscale modeling and nested simulations of three-dimensional ionospheric plasmas. *Phys Scr* 89:098001.
11 Peters N (2000) *Turbulent Combustion* (Cambridge Univ Press, Cambridge, UK).
12 Zeldovich YB, Raizer YP (2002) *Physics of Shock Waves and High-Temperature Hydrodynamic Phenomena* (Dover, New York).
13 Prosperetti A, Plesset MS (1984) The stability of an evaporating liquid surface. *Phys Fluids* 27:1590–1602.
14 Zhakhovsky VV, Kryukov AP, Levashov VY, Shishkova IN, Anisimov SI (2018) Mass and heat transfer between evaporation and condensation surfaces: Atomistic simulation and solution of Boltzmann kinetic equation. *Proc Natl Acad Sci USA,* 201714503.
15 Rana S, Herrmann M (2011) Primary atomization of a liquid jet in crossflow. *Phys Fluids* 23:091109.
16 Wu PK, et al. (1997) Breakup processes of liquid jets in subsonic crossows. *J Propuls Power* 13:64–73.
17 Orlov SS, Abarzhi SI, Oh SB, Barbastathis G, Sreenivasan KR (2010) High-performance holographic technologies for fluid-dynamics experiments. *Philos Trans A Math Phys Eng Sci* 368:1705–1737.
18 Kadau K, Barber JL, Germann TC, Holian BL, Alder BJ (2010) Atomistic methods in fluid simulation. *Philos Trans A Math Phys Eng Sci* 368:1547–1560.
19 Glimm J, Li XL, Liu Y, Zhao N (2001) Conservative front tracking and level set algorithms. *Proc Natl Acad Sci USA* 98:14198–14201.
20 Abarzhi SI, Fukumoto Y, Kadanoff LP (2015) Stability of a hydrodynamic discontinuity. *Phys Scr* 90:018002.
21 Kadanoff LP (2000) *Statistical Physics–Statistics, Dynamics and Renormalization* (World Scientific, Hackensack, NJ).
22 Lord R (1883) Investigations of the character of the equilibrium of an incompressible heavy fluid of variable density. *Proc Lond Math Soc* 14:170–177.
23 Davies RM, Taylor GI (1950) The mechanics of large bubbles rising through extended liquids and through liquids in tubes. *Proc R Soc Lond A Math Phys Sci* 200:375–390.
24 Richtmyer RD (1960) Taylor instability in shock acceleration of compressible fluids. *Commun Pure Appl Math* 13:297–319.
25 Meshkov EE (1969) Instability of the interface of two gases accelerated by a shock. *Sov Fluid Dyn* 4:101–104.
26 Meshkov EE (2006) [*Studies of Hydrodynamic Instabilities in Laboratory Experiments*] (FGYC-VNIIEF, Sarov, Russia). Russian.
27 Chandrasekhar S (1981) *Hydrodynamic and Hydromagnetic Stability* (Dover, New York).
28 Nishihara K, Wouchuk JG, Matsuoka C, Ishizaki R, Zhakhovsky VV (2010) Richtmyer-Meshkov instability: Theory of linear and nonlinear evolution. *Philos Trans A Math Phys Eng Sci* 368:1769–1807.
29 Wouchuk JG (2001) Growth rate of the linear Richtmyer-Meshkov instability when a shock is reflected. *Phys Rev E Stat Nonlin Soft Matter Phys* 63:056303.
30 Abarzhi SI (2008) Review on nonlinear coherent dynamics of unstable fluid interface: Conservation laws and group theory. *Phys Scr* T132:297681.
31 Abarzhi SI, Nishihara K, Rosner R (2006) Multiscale character of the nonlinear coherent dynamics in the Rayleigh-Taylor instability. *Phys Rev E Stat Nonlin Soft Matter Phys* 73:036310.
32 Bodner SE (1974) Rayleigh–Taylor instability and laser-pellet fusion. *Phys Rev Lett* 33:761–764.
33 Remington BA, et al. (1995) Single mode and multimode Rayleigh-Taylor experiments on Nova. *Phys Plasmas* 2:241–255.
34 Azechi H, et al. (2007) Comprehensive diagnosis of growth rates of the ablative Rayleigh-Taylor instability. *Phys Rev Lett* 98:045002.
35 Hurricane OA, et al. (2014) The high-foot implosion campaign on the National Ignition Facility. *Phys Plasmas* 21:056314.
36 Willcox DE, et al. (2016) Type Ia supernova explosions from hybrid carbon-oxygen-neon white dwarf progenitors. *Astrophys J* 832:1–14.
37 Markstrein GH (1964) *Nonsteady Flame Propagation* (Pergamon, Oxford).
38 Williams FA (1965) *Combustion Theory* (Addison-Wesley, Reading, MA).
39 Williams FA (1971) Theory of combustion in laminar flows. *Annu Rev Fluid Mech* 3:171–288.
40 Landau LD (1944) On the theory of slow combustion. *Acta Physicochim URSS* 19:77–85.
41 Kull HJ, Anisimov SI (1986) Ablative stabilization in the incompressible Rayleigh–Taylor instability. *Phys Fluids* 29:2067–2075.
42 Sanz J (1994) Self-consistent analytical model of the Rayleigh-Taylor instability in inertial confinement fusion. *Phys Rev Lett* 73:2700–2703.
43 Aglitskiy Y, et al. (2010) Basic hydrodynamics of Richtmyer-Meshkov-type growth and oscillations in the inertial confinement fusion-relevant conditions. *Philos Trans A Math Phys Eng Sci* 368:1739–1768.
44 Sivashinsky GI (1983) Instabilities, pattern formation, and turbulence in flames. *Annu Rev Fluid Mech* 15:179–199.
45 Liberman MA, Bychkov VV, Golberg SM, Book DL (1994) Stability of a planar flame front in the slow-combustion regime. *Phys Rev E Stat Phys Plasmas Fluids Relat Interdiscip Topics* 49:445–453.
46 Ilyin DV, Goddard III WA, Cheng T (2018) First principles based reaction kinetics from reactive molecular dynamics simulations. *Proc Natl Acad Sci USA*, 10.1073/pnas.1701383115.
47 Beklemishev DV (1971) *Course of Analytical Geometry and Linear Algebra* (Nauka, Moscow).
48 D'yakov SP (1954) Ob ustoichivosti udarnyh voln. *Zh Exp Teor Fiz* 27:288–295.
49 Kontorovich VM (1958) Concerning the stability of shock waves. *Sov Phys JETP* 6:1179–1180.